

## Article

# Seismic Vulnerability Analysis of Masonry Structures Built with Disassembled Brick Wall Sections

Zhiming Su <sup>1</sup>, Wenzhong Zheng <sup>1,2,3,\*</sup>, Ying Wang <sup>1,2,3</sup> and Xiaomeng Hou <sup>1,2,3</sup> <sup>1</sup> School of Civil Engineering, Harbin Institute of Technology, Harbin 150090, China<sup>2</sup> Key Laboratory of Structures Dynamic Behaviour and Control of the Ministry of Education, Harbin Institute of Technology, Harbin 150090, China<sup>3</sup> Key Laboratory of Smart Prevention and Mitigation of Civil Engineering Disasters of the Ministry of Industry and Information Technology, Harbin Institute of Technology, Harbin 150090, China

\* Correspondence: zhengwenzhonghit@126.com

**Abstract:** Disassembling brick wall pieces into brick wall sections and constructing masonry buildings with disassembled brick wall sections (DBWSs) can reduce construction waste production at source and help achieve carbon peak and carbon neutrality. A finite element model (FEM) for typical MSBD is established based on the calibrated finite element analysis method to evaluate the seismic performance of masonry structures built with disassembled brick wall sections (MSBD). Subsequently, the peak ground acceleration is selected as the ground motion intensity index, and the maximum inter-story displacement angle is chosen as the structural damage index. The 20 ground motion records are selected and scaled by peak acceleration in 0.2 g steps to form 120 structure-ground vibration samples for incremental dynamic analysis (IDA) and seismic vulnerability analysis. The IDA results indicated that with the gradual increase in peak ground acceleration, the maximum inter-story displacement angle increases and the model transits from the elastic stage to the elastoplastic stage. Because the characteristics of ground motion records are different, the order of structural plasticity development will be different and the number of ground motion records needs to be considered in the seismic performance assessment. The calculation model will not collapse under the 7 and 8 degree design-based earthquake and the probability of moderate and severe damage of the structure under the rare earthquake is minimal, according to the seismic vulnerability curves. The seismic vulnerability analysis results indicate that MSBD has good seismic performance under earthquakes and meets the requirements of “perfect subjected to frequent earthquake, reparable subjected to design based earthquake, no collapse subjected to rare earthquake.” The seismic vulnerability analysis based on probability statistics can provide a reference for seismic design and evaluation of earthquake damage.

**Keywords:** DBWSs; MSBD; reutilization; seismic performance; vulnerability analysis

**Citation:** Su, Z.; Zheng, W.; Wang, Y.; Hou, X. Seismic Vulnerability Analysis of Masonry Structures Built with Disassembled Brick Wall Sections. *Buildings* **2022**, *12*, 1831. <https://doi.org/10.3390/buildings12111831>

Academic Editor: Marco Di Ludovico

Received: 12 October 2022

Accepted: 25 October 2022

Published: 1 November 2022

**Publisher's Note:** MDPI stays neutral with regard to jurisdictional claims in published maps and institutional affiliations.



**Copyright:** © 2022 by the authors. Licensee MDPI, Basel, Switzerland. This article is an open access article distributed under the terms and conditions of the Creative Commons Attribution (CC BY) license (<https://creativecommons.org/licenses/by/4.0/>).

## 1. Introduction

Due to its advantages in terms of easy production, straight forward construction, and durability, clay bricks are frequently employed in civil building projects worldwide. China issued a ban on the production and use of clay bricks in 2004 to save energy and land resources [1]. With the rapid development of society, some masonry structures are facing the situation of renovation or demolition, owing to the function that does not meet the requirements of modern society, the seismic fortification level that does not meet the current standards and the need for urban reconstruction, etc. [2–5]. However, the quality of the brick walls of the masonry houses that are planned to be demolished may still be good, and most of the demolished materials are treated as construction wastes [6], which is incompatible with the road of green development of construction projects. At present, countries, such as China and Germany, are vigorously building a circular economy system [7]. In this context, the dismantling and reuse of brick wall sections can reduce the production of construction waste at source and help achieve carbon peaking and carbon

neutrality [8]. One method of reusing masonry structural elements is to recover bricks of good quality. This method is largely driven by the specific high-value or unique vintage look of the bricks [9]. Another method of reusing masonry structural elements is to crush and grind bricks and mortar blocks to a certain fineness. Brick powder of certain fineness has pozzolanic activity and hydration activity [10,11], which can be used as an admixture to reduce the amount of cement. This method can reduce resource consumption and environmental pollution caused by cement production.

In addition, using disassembled brick wall sections (DBWSs) to build new masonry structures is an effective method. The notion of employing well-preserved brick wall parts to build new masonry homes introduced by the Cubo project [12], which focuses on the renovation of residential houses. Zhou [13] analyzed the mechanical properties of the disassembled bricks and the brick wall specimens made from the disassembled bricks. It was stated that the disassembled process had little effect on the masonry properties, and its bearing capacity calculation could also be carried out regarding the current code. Ucer [14] obtained the DBWSs from the demolition site and tested the mechanical properties. The strength of the bricks and wall sections was found to be more than the current code's minimal requirement, and the bonds between brick and mortar were good. In other words, the DBWSs can be used to build new houses, provided proper design methods are used.

The seismic performance of masonry structures is significantly influenced by the performance of the brick walls and linkages between walls and structural columns. Nevertheless, for seismic performance, most existing studies focus on reinforced masonry structures and masonry structures built with new materials. Additionally, little attention has been paid to the research on the seismic performance of masonry structures built with disassembled brick wall sections (MSBD). Compared with usual masonry structures, the spacing between constructional columns of MSBD is smaller. It is worth evaluating the seismic performance of buildings with MSBD characteristics. Accurate seismic vulnerability analysis is a necessary condition for reliable prediction in seismic risk assessment. In the previous studies, four vulnerability analysis methods were proposed, including the expert judgment method, empirical analysis method, theoretical analysis method, and mixed analysis method [15,16]. The advantage of the theoretical analysis method is using numerical simulations for the study, which is not limited by specific conditions and can analyze the vulnerability of structures lacking research data.

Therefore, this paper proposed a modeling method of MSBD based on Abaqus software and confirmed the validity of the finite element analysis methods. Based on the usual MSBD, a simplified five-story masonry cross wall was created as the calculation model and 20 ground motion records were chosen for nonlinear incremental dynamic analysis (IDA). Based on the IDA curves and the structural performance level, the seismic vulnerability curves of the calculation model can be created. The seismic capacity of the structure can be determined according to the conditional probability of the structure reaching each limit state, which can serve as a guide for seismic design and earthquake damage assessment.

## 2. Masonry Structures Built with DBWSs

To ensure the durability and seismic performance of MSBD, the brick wall sections without surface damage in a dry and low erosive environment should be selected as the objects for disassembling, and the mechanical properties of the DBWSs should be examined. The actual size of the wall pieces, the permitted size of the transport trucks, the lifting capacity of the lifting equipment, etc., should be considered when determining the size of the DBWSs. The width of the DBWSs is recommended to be 1.0~4.8 m and the height of the DBWSs is recommended to be 0.9~3.6 m, according to GB 50003-2011 [17] and 18CG40 + 18CJ79-1 [18].

Wall components for brick masonry houses comprise both wall pieces and wall pieces with cavities. The roof slab of the floor on which the brick wall to be cut is disassembled must first be removed before the brick wall pieces may be divided into brick wall sections. For brick wall components without cavities, the cutting strategy should be chosen based on



the DBWSs and the constructional column, ensuring the continuity of load transfer. The L-shaped connection and T-shaped connection between the DBWSs can be completed by referring to the above method.

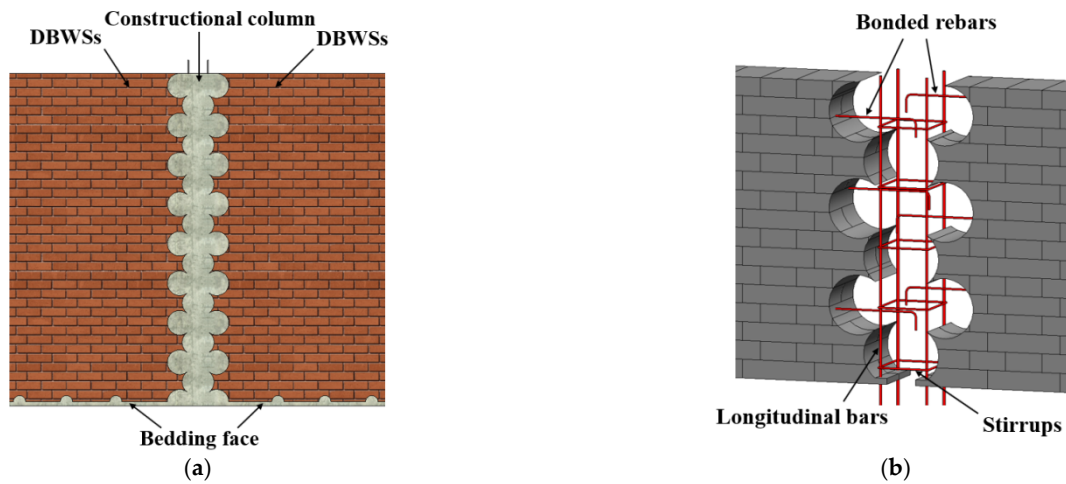


**Figure 2.** Construction details: (a) horizontal connection between the DBWSs; (b) the reinforcement configuration at vertical joints details.

### 3. Finite Element Models

#### 3.1. General Strategy

In this section, the numerical simulation of the masonry structure model is carried out using the finite element analysis program ABAQUS. Generally speaking, masonry wall modeling approaches are classified into integral modeling and separated modeling [19]; the choice depends on the accuracy required for the study. The integral modeling approach treats masonry as homogeneous material and models masonry walls as a series of continuous units [20], as shown in Figure 3a. It is more advantageous in modeling relatively large and complex masonry walls. This method, however, cannot be used to describe precise failure modes. The separated modeling approach in Figure 3b considers elements, mortars, and interfaces to provide accurate results. However, the applicability of this method in the analysis of large masonry buildings is constrained by the high computational cost [20]. Alternatively, a simplified separated modeling approach in Figure 3c can be used to simplify calculation costs, which reduces mortar joints to non-thickness interfaces, and half of the mortar's thickness was added to the element's thickness to take into account the mortar's thickness. The accuracy of the simulation findings could be slightly affected by this streamlined approach, but researchers still heavily favor this approach because of the huge cost savings [21].

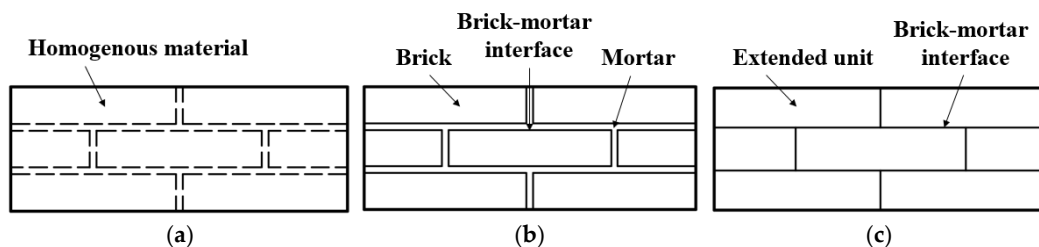


**Figure 3.** Modeling approaches: (a) separated modeling approach; (b) integral modeling approach; (c) simplified separated modeling approach [22].

#### 3.2. Calibration of the Finite Element Model (FEM)

Recently, an experimental study on in-plane static cyclic loading of a two-story masonry structure model built with the DBWSs has been carried out. The findings of this study

in terms of force–displacement curves and observed failure modes were used to confirm the validity of the finite element analysis methods. The simplified separated modeling approach was used to establish the FEM of MSBD. Due to masonry walls' highly nonlinear and brittle characteristics, a dynamic explicit solver was selected as the numerical solving method. A dynamic explicit solver does not require an assembly matrix, which makes it easy to solve complex contact problems, compared to the standard solver. As the model grows, dynamic explicit solver requires fewer resources than standard solver. It should be noted that the dynamic explicit solver essentially uses slow loading to model static problems that require increased computation time to reduce the effect of inertial forces. Generally, quasi-static analysis can be accomplished by taking more than 10 times the period corresponding to the structure's lowest order modal. Simultaneously, the kinetic energy and internal energy of the model must be assessed. When the material's kinetic energy does not exceed 10% of the internal energy, the loading process can essentially be ensured to be quasi-static [23].

### 3.2.1. Material Constitutive Model

The objects of finite element analysis are masonry walls with structural columns, including extended units of bricks and mortar, concrete and reinforcement. Due to its capability of taking into account the fully inelastic behavior of concrete in compression and tension, the concrete damaged plasticity (CDP) model in ABAQUS can be used to study the mechanical properties of brittle materials, such as concrete and masonry, under uniaxial loading or cyclic loading [21,24]. For masonry modeling, Yang [25] and Sekender Ali [26] produced a model that was considered for stress–strain relationship and was presented in Figure 4. Yang [25] established the masonry uniaxial compressive stress–strain relationship based on the unitary equilibrium condition through a mesoscopic model. Yang model [25] can be stated as:

$$\frac{\sigma_c}{f_{cm}} = \frac{\eta}{1 + (\eta - 1) \left(\frac{\varepsilon_c}{\varepsilon_{cm}}\right)^{\eta/(\eta-1)}} \frac{\varepsilon_c}{\varepsilon_{cm}} \quad (1)$$

where  $\sigma_c$  is the compression stress of masonry;  $\varepsilon_c$  is the compression strain of masonry;  $f_{cm}$  is the peak compression stress of masonry;  $f_{cm} = 0.78f_1^{0.5}(1 + 0.07f_2)$  where  $f_1$  is the average compressive strength of bricks,  $f_2$  is the average compressive strength of mortar;  $\varepsilon_{cm}$  is the peak compression strain of masonry;  $\varepsilon_{cm} = 0.005/\sqrt{f_{cm}}$  where  $\eta$  is the ratio of the initial tangential modulus to the peak cutline modulus, generally taken as 1.633.

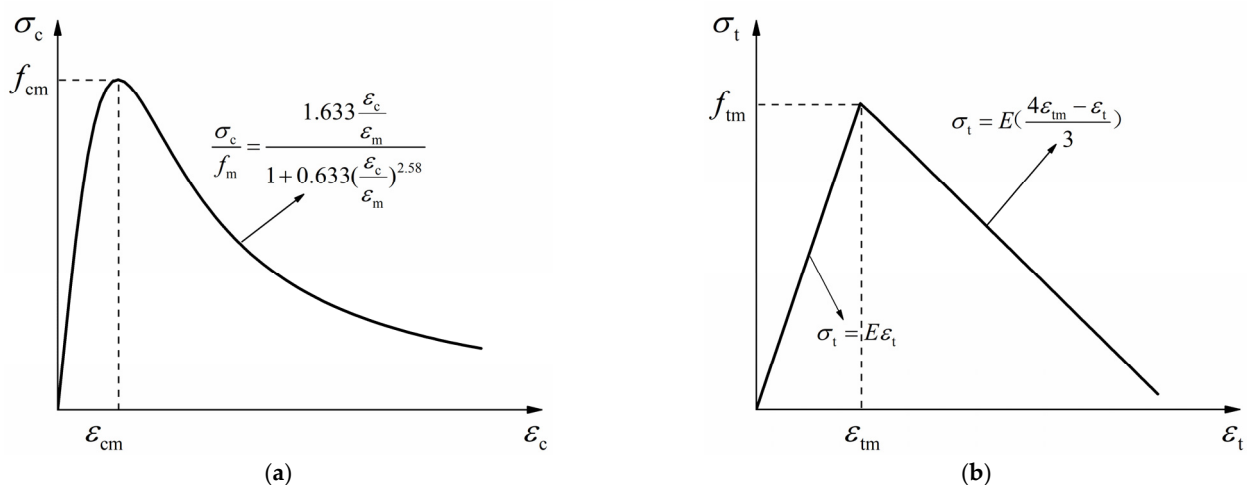


**Figure 4.** Stress–strain relationships used for masonry: (a) Compressive behavior based on Yang model [25]; (b) Tensile behavior based on Sekender Ali model [26].

Sekender Ali [26] used a simplified bilinear model to describe the uniaxial tensile stress–strain relationship in masonry. Sekender Ali [26] model can be expressed, as shown in Equation (2):

$$\sigma_t = \begin{cases} E\varepsilon_t, & \varepsilon_t \leq \varepsilon_{tm} \\ \frac{E(4\varepsilon_{tm}-\varepsilon_t)}{3}, & \varepsilon_{tm} < \varepsilon_t \leq 4\varepsilon_{tm} \end{cases} \quad (2)$$

where  $\sigma_t$  is the tension stress of the masonry;  $\varepsilon_t$  is the tension strain of the masonry;  $\varepsilon_{tm}$  is the peak tension strain of the masonry;  $E$  is the elastic modulus of masonry;  $E = 370f_{cm}\sqrt{f_{cm}}$ .

Extended units of bricks and mortar modeling are considered as an integral model of bricks and mortar, except that the weak layer of masonry is modeled by an interface model. Thus, the stress–strain relationship of masonry is still used in the simplified separated model for the extended units. The Poisson’s ratio of masonry and the extended units was set as 0.15.

For concrete modeling, the uniaxial stress–strain relationships used for concrete proposed by GB50010-2010 were considered. The Poisson’s ratio of concrete was set as 0.2. Damage factors for both masonry and concrete were calculated based on the Sidoroff energy equivalence principle [27]. The bilinear elastic–plastic stress–strain model with strain hardening was taken into consideration for modeling steel reinforcement, and it is shown in Figure 5. Based on the results of the material testing, the steel reinforcement’s parameters were established, and the Poisson’s ratio was set at 0.3.

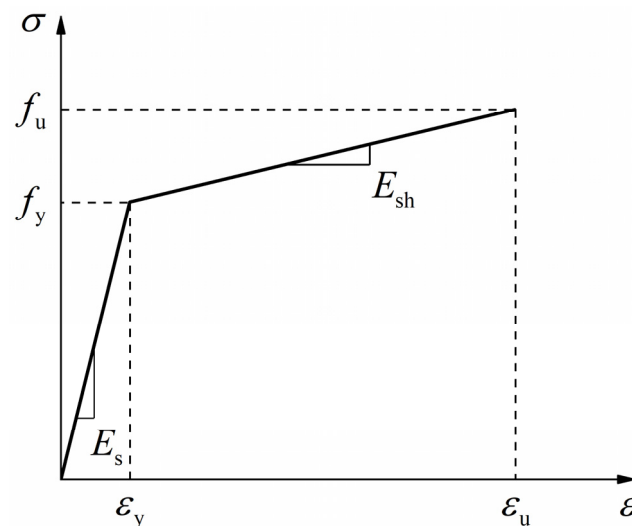


Figure 5. Stress–strain relationships used for steel reinforcement.

### 3.2.2. Modelling Approach

The FEM in simplified separated modeling was composed of extended units, concrete columns, concrete foundation beams, concrete slabs, and steel reinforcements. The C3D8R was used for extended units, concrete foundation beams, and concrete slabs. The T3D2 was used for steel reinforcements. The proper FEM mesh size was chosen based on the mesh sensitivity analysis. The global mesh size of the FEM was set to 60, and the sweeping approach was employed. The “Tie” constraint was used to establish the interaction between extended units, concrete columns, concrete foundation beams, concrete slabs. The relationship between concrete columns and steel reinforcements was established via the “Embedded” constraint.

Under horizontal loads, the damage to masonry usually occurs at the mortar interface, which has a certain tensile and shear strength, and the adjacent part has a friction effect after the joint interface is damaged. It is possible to accurately simulate the shear behavior of masonry by modeling the joint interfaces between the expanded units using a surface-based cohesive approach [28]. The interaction between the expanded units was modeled using the “General” contact. The cohesive interface model is a bilinear constitutive model, which

is based on a bilinear traction separation model in tension and shear in ABAQUS [29]. The interface strength begins to degrade once the specified ultimate strength is reached in the traction separation model, which initially exhibits a linear elastic behavior. Using the laws of initial damage and damage evolution in contact properties, the mechanical properties of degradation can be simulated. The traction separation model [30] can be expressed, as shown in Equation (3):

$$t = \begin{Bmatrix} t_n \\ t_s \\ t_t \end{Bmatrix} = \begin{bmatrix} k_{nn} & 0 & 0 \\ 0 & k_{ss} & 0 \\ 0 & 0 & k_{tt} \end{bmatrix} \begin{Bmatrix} \delta_n \\ \delta_s \\ \delta_t \end{Bmatrix} = \mathbf{K}\delta \quad (3)$$

where  $t_n^{\max}$ ,  $t_s^{\max}$ ,  $t_t^{\max}$  are the ultimate traction forces in the linear elastic phase, respectively, which are usually taken as the tensile and shear strength of the mortar;  $\delta_n^0$ ,  $\delta_s^0$ ,  $\delta_t^0$  are the corresponding displacements;  $\mathbf{K}$  is the stiffness matrix of joint interfaces;  $k_{nn} = \frac{E_u E_m}{h_m (E_u - E_m)}$ ,  $k_{ss} = k_{tt} = \frac{G_u G_m}{h_m (G_u - G_m)}$  where  $E_u$  is the elastic modulus of brick,  $E_m$  is the elastic modulus of mortar,  $G_u$  is the shear modulus of brick,  $G_m$  is the shear modulus of mortar,  $h_m$  is the thickness of mortar. The critical mixed-mode fracture energy needed to destroy joint surfaces can be seen as the darkened area in Figure 6, which is based on the Benzeggagh–Kenane law. The normal and tangential fracture energies can be calculated from the interfacial tensile and shear strength due to the difficulty in measuring fracture energies in tests [28,31]. The maximum traction forces, the stiffness matrix, and the critical mixed-mode fracture energy determine the cohesive interface model.

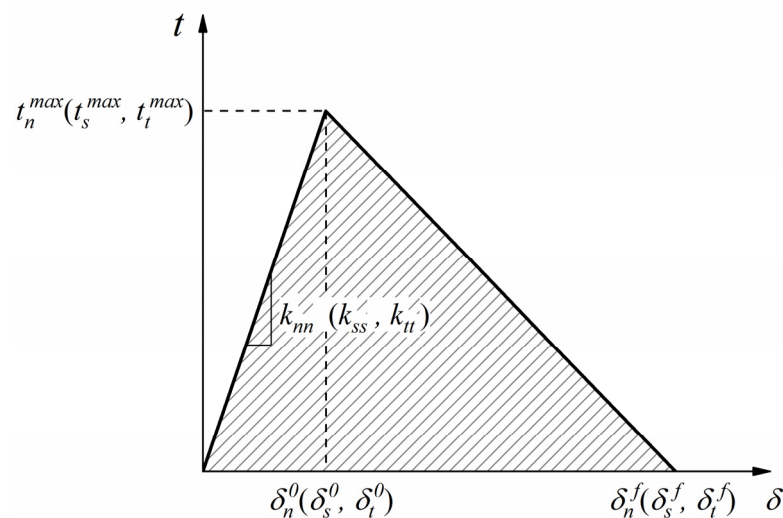


**Figure 6.** Traction separation model [30].

### 3.2.3. Comparison with Experimental Results

The experimental study on in-plane static cyclic loading of a two-story masonry structure model built with the DBWSs was performed at the structural and seismic laboratory of Harbin Institute of Technology. Due to the limitation of the test site and loading device, the model plane size was determined as 3.24 m × 3.24 m, the wall thickness was 240 mm, the height of the 1st floor was 2.0 m, and the height of the 2nd floor was 1.7 m. The dimension of bricks used in the DBWSs was 240 mm × 115 mm × 53 mm. All the DBWSs and columns were built over reinforced concrete foundation beams and bolted to a strong and rigid floor designed to prevent the experimental model from moving during cyclic loading.

The material properties used for masonry in the FEM, especially compressive strength, shear strength, density, and elasticity modulus, shall be determined by referring to GB 50003-2011 [17], GB/T 50129-2011 [32], and GB/T 50315-2011 [33]. Other properties, including concrete's compressive strength, tensile strength, density, and elasticity modulus, were

determined by referring to GB 50010-2010 [34]. The mechanical properties of masonry, concrete, and steel used in the FEM are shown in Table 2.

**Table 2.** Mechanical properties of materials.

Material	Property	Value
Masonry	Compressive strength	3.40 MPa
	Shear strength	0.304 MPa
	Modulus of elasticity	2320 MPa
	Density	2000 kg/m <sup>3</sup>
	Poisson's ratio	0.15
Concrete	Compressive strength	23.41 MPa
	Tensile strength	2.57 MPa
	Modulus of elasticity	29,254 MPa
	Density	2500 kg/m <sup>3</sup>
	Poisson's ratio	0.2
Steel	Yield strength of HPB300	346 MPa
	Yield strength of HRB400	485 MPa
	Modulus of elasticity	210,000 MPa
	Density	7850 kg/m <sup>3</sup>
	Poisson's ratio	0.3

In the CDP model, it is also necessary to specify the relevant material parameters to define the plastic flow potential function and yield surface accurately. The default values for flow potential eccentricity ( $\varepsilon = 0.1$ ), the ratio between biaxial and uniaxial compressive yield stress ( $f_{b0}/f_{c0} = 1.16$ ), the ratio between the second stress invariants on the tensile and the compressive meridians ( $K = 2/3$ ), and the viscosity parameter ( $\mu = 0.001$ ) were determined, according to the Abaqus user's manual [35] and previous studies [30,36–41]. In addition, to correctly simulate masonry behavior during the calibration process, the dilation angles of 36° and 20° for concrete and masonry materials were considered.

Due to the symmetry of load and geometry of the studied masonry structure model built with the DBWSs, only one-half model was built to improve computational efficiency in the current study. For boundary conditions, the displacements of the 1st and 2nd floor slab in X rotation, Y translation, and Z rotation were restricted. For the loading method, unidirectional displacement loading is applied to the reference point to consider the computational efficiency, coupled to the top surface of the 2nd floor slab. The vertical loads were applied to the 1st and 2nd floor slab, resulting in vertical stress of 0.5 MPa for the 2nd floor walls and 0.6 MPa for the 1st floor walls, as illustrated in Figure 7. The damage of the floor slab was not considered; only the part in contact with the wall pieces was created and set as a rigid body.

Figure 8a,b represent the damage distribution between the experimental model and the FEM. In terms of failure and cracking mode, the FEM results were found to be in good agreement with the experimental results. In addition, the force–displacement curves of the FEM and the experimental model were compared in Figure 8c. The force–displacement curves were nearly identical; however, the FEM's stiffness of the rising phase of the force–displacement curve was slightly greater than that of the experimental model. The differences are related to the loading method and the assumptions of the material constitutive model. Low-cyclic reversed loading was used in the experimental model. The accumulation of compressive and tensile damage under cyclic loading led to a decrease in the stiffness of the experimental model, and the assumption of homogeneous materials

was equivalent to enhancing the mechanical properties of materials. However, the FEM was unable to account for the aforementioned factors temporarily.

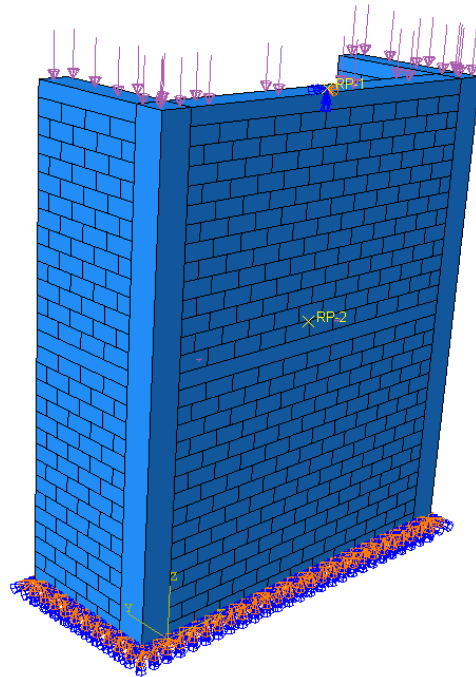
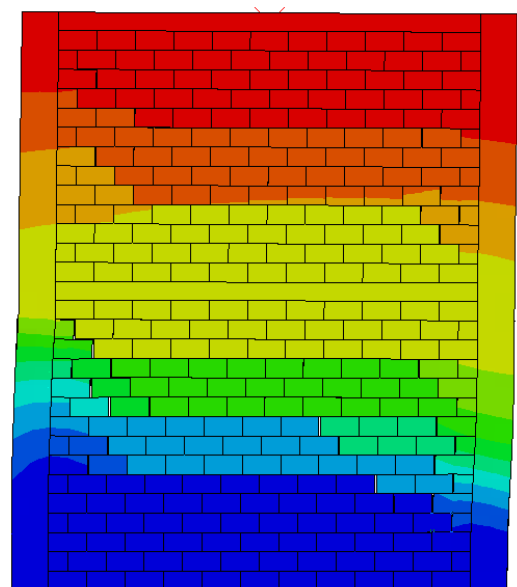


Figure 7. One-half model of MSBD.

The stiffness, strength, and ductility of the experimental model were generally accurately represented by the simplified separated FEM, demonstrating the applicability of the methods and assumptions used in the finite element modeling, which will be implemented in the subsequent seismic vulnerability analysis.



(a)



(b)

Figure 8. Cont.

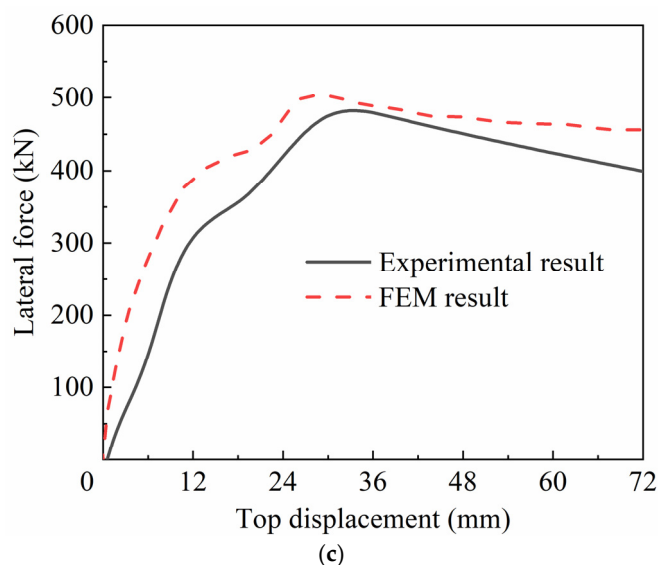


**Figure 8.** Comparison between the cracking modes and force–displacement curves of the experimental and FEM results: (a) cracking pattern of experimental results; (b) lateral displacement contour of numerical modeling results; (c) force–displacement curves.

#### 4. Seismic Vulnerability Analysis for MSBD

The seismic vulnerability analysis of buildings can predict damage before earthquakes and help designers improve structures' seismic performance [16]. It can also be used to evaluate the losses after earthquakes and provide a basis for disaster estimation, relief, and reconstruction. IDA can reflect the change process of strength, stiffness, and deformation capacity of structures under different ground motions, which can be used to analyze the vulnerability of MSBD [42]. Furthermore, IDA can forecast the probability of damage at different degrees of earthquake activity, which can establish a rationale for seismic performance assessment based on scientific data.

##### 4.1. FEM for Seismic Vulnerability Analysis

In this paper, the masonry structure model built with the DBWSs was simplified as a three-dimensional masonry wall piece for analysis, since only the in-plane failure mechanism of masonry structures was concerned, and the out-of-plane failure mechanism was not considered for the time being. The influence of DBWSs dimensions on the seismic performance of brick masonry structures should be taken into consideration in the structural design, compared to conventional masonry structures. Therefore, a five-story masonry crosswall was designed as the calculation model for vulnerability analysis. The thickness of crosswall was 240 mm, the width of each DBWSs was 3.0 m, and the height of each floor was 3.0 m. The dimensions of structural columns and ring beams were 240 mm × 240 mm and 180 mm × 240 mm, respectively. The thickness of the concrete protective layer of structural columns and ring beams was 20 mm, and the reinforcement was configured according to the structure. All parameters of the computational model were determined to meet the GB50003-2011 [17] requirements.

The calculation model was built the same way as in Section 3.2, and the material parameters were the same as in Table 2. A vertical load of 0.2 MPa was applied to the ring beam of each floor. For the computational model, it should be noted that when all wall parts are built using the separated modeling approach and considering the contact between units, the modeling and computational workloads will be relatively large, and appropriate simplification of the computational model can be considered. Therefore, the DBWSs were established with a height of 1.41 m, and only the contact between DBWSs was considered, as shown in Figure 9.

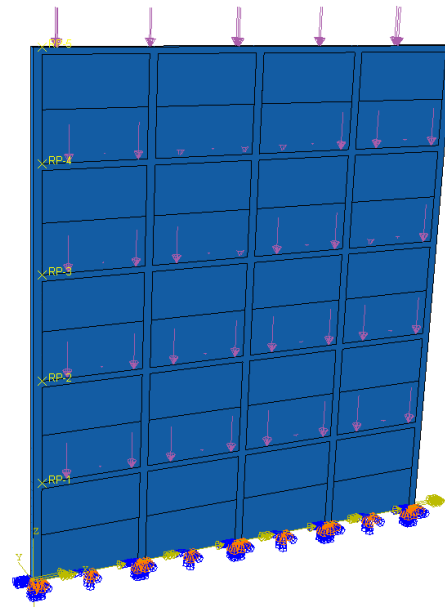


**Figure 9.** Calculation model.

#### 4.2. Selection of Ground Motion Records

According to Riddell's study [43], the correlation of the peak ground acceleration index decreased with increasing structural period and was applicable to short-period building structures. The period of masonry buildings was generally not higher than 0.4 s, a short-period structure. Further, the seismic hazard levels in GB50011-2011 [44] were prescribed in terms of peak ground acceleration; hence, the peak ground acceleration ( $A_{pg}$ ) was selected as the ground motion intensity index. To reduce the impact of ground motion uncertainty on the seismic vulnerability analysis, 20 ground motion records were selected from the strong shaking record database of the Pacific Earthquake Research Center, regarding the wave selection principles suggested in the FEMA-P695 [45], as shown in Table 3. The selected seismic records' average response spectrums generally agree with the Chinese code design response spectrum [44], as presented in Figure 10.

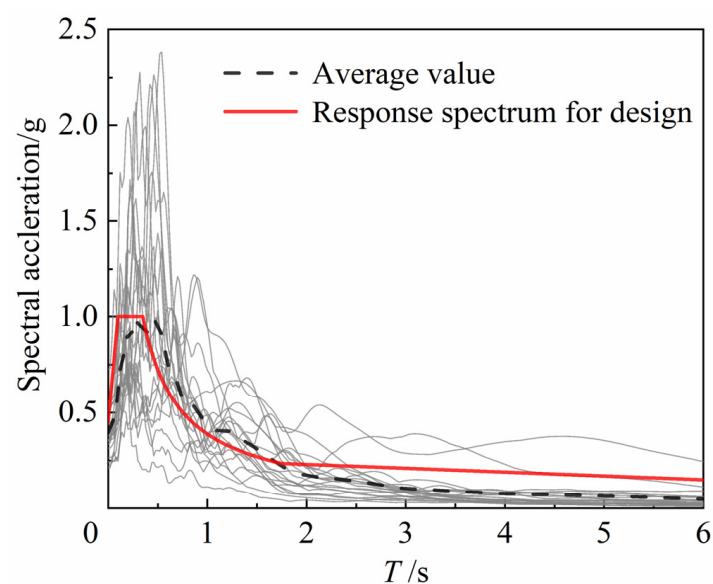


**Figure 10.** Response spectrums.

**Table 3.** The selected ground motion records.

Earthquake Name	Record Sequence Number	Peak Ground Acceleration	Earthquake Name	Record Sequence Number	Peak Ground Acceleration
San_Fernando	PEL090	0.21 g	Northridge-01	MUL279	0.52 g
Friuli-Italy	TMZ270	0.31 g	Kobe-Japan	NIS000	0.51 g
Imperial_Valley	DLT352	0.35 g	Kobe-Japan	SHI000	0.24 g
Imperial_Valley	E11230	0.38 g	Kocaeli-Turkey	ARC000	0.22 g
Superstition_Hills	ICC000	0.36 g	Kocaeli-Turkey	DZC270	0.36 g
Loma_Prieta	CAP000	0.53 g	ChiChi	CHY101E	0.35 g
Loma_Prieta	G03000	0.56 g	ChiChi	CHY101N	0.44 g
Cape_Mendocino	RIO360	0.55 g	Duzce-Turkey	BOL000	0.73 g
Landers	CLW-TR	0.42 g	Hector_Mine	HEC000	0.27 g
Landers	YER270	0.24 g	Hector_Mine	HEC090	0.34 g

#### 4.3. Judgment of Structural Performance Level

The applicability and accuracy of the structural damage index directly affect the shape of the vulnerability curve and conditional exceedance probability. Displacement indexes are mainly adopted for seismic vulnerability analysis, including maximum inter-story displacement angle and maximum inter-story displacement [46,47]. The maximum inter-story displacement angle ( $\theta_{max}$ ) can reflect the influence of factors, such as structural form, material, story height, and damage; thus, it is selected as the structural damage index.

The performance level cutting point on the IDA curves should be identified to evaluate the seismic performance of structures during earthquakes. Based on the three-level fortification requirements of GB50011-2010 [44], the recommendations of FEMA [48] and previous studies [46,49–51], the performance level of masonry structure was divided into four grades, operational (OP), immediate occupancy (IO), life safety (LS) and collapse prevention (CP). The inter-story displacement angle limits of each performance level are shown in Table 4.

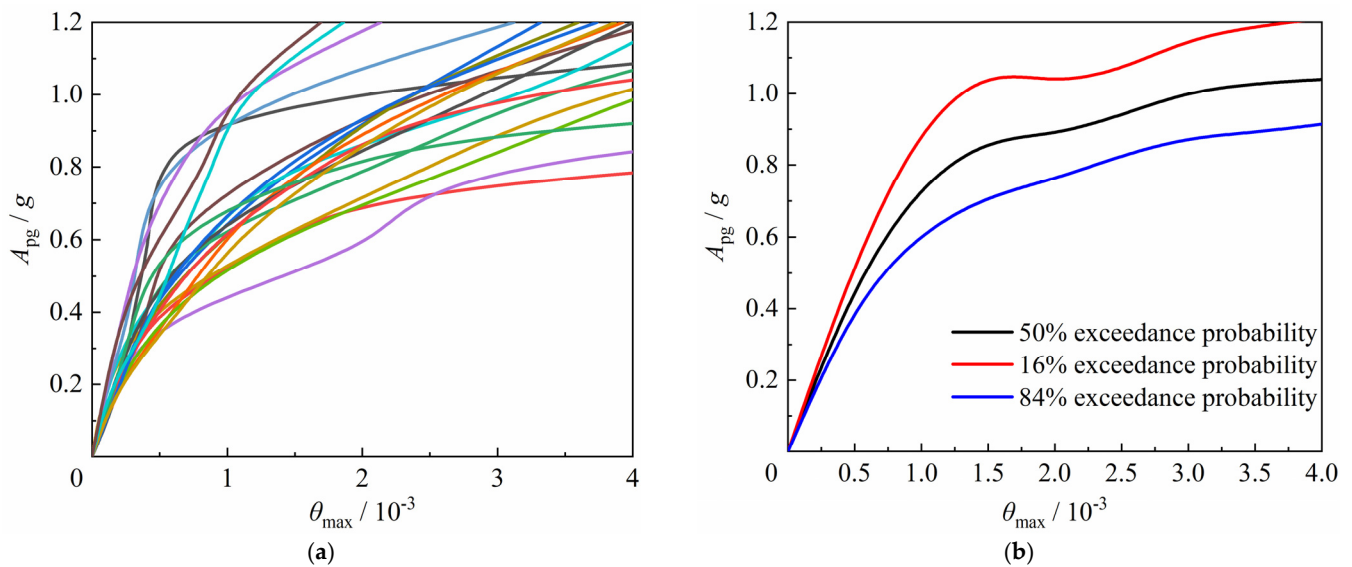
**Table 4.** Inter-story displacement angle limits of each performance level.

Performance levels	Operational	Immediate Occupancy	Life Safety	Collapse Prevention
Damage state	Slight damage	Moderate damage	Severe damage	Collapse
Inter-story displacement angle	0.0005	0.0011	0.0018	0.0029

#### 4.4. Seismic Vulnerability Curve

The 20 ground motion records selected previously were scaled by peak acceleration in 0.2 g steps to form 120 structure–ground vibration samples. The maximum inter-story displacement angle for different ground motion intensities can be determined utilizing Abaqus to conduct elastic–plastic time–history analysis on the calculation model. After multiple calculations and integration of relevant data, 20 IDA curves can also be obtained. Statistical methods were used to measure the analysis results of IDA curves [52], and the 16%, 50%, and 84% exceedance probability curves of the overall analysis results are illustrated in Figure 11.

As can be seen from Figure 11, when the peak ground acceleration was small, the model was in the elastic stage, and the IDA curves exhibited a monotonic increasing trend. The model entered the elasto-plastic stage and damage intensification and stiffness degradation began, and the IDA curves displayed a non-monotonic increasing trend as the peak ground acceleration gradually increased. When the model was seriously damaged, 16% of the 20 ground motion records had a peak acceleration of no more than 1.18 g, 50% had a peak acceleration of no more than 1.02 g, and 84% had a peak acceleration of no more than 0.88 g.



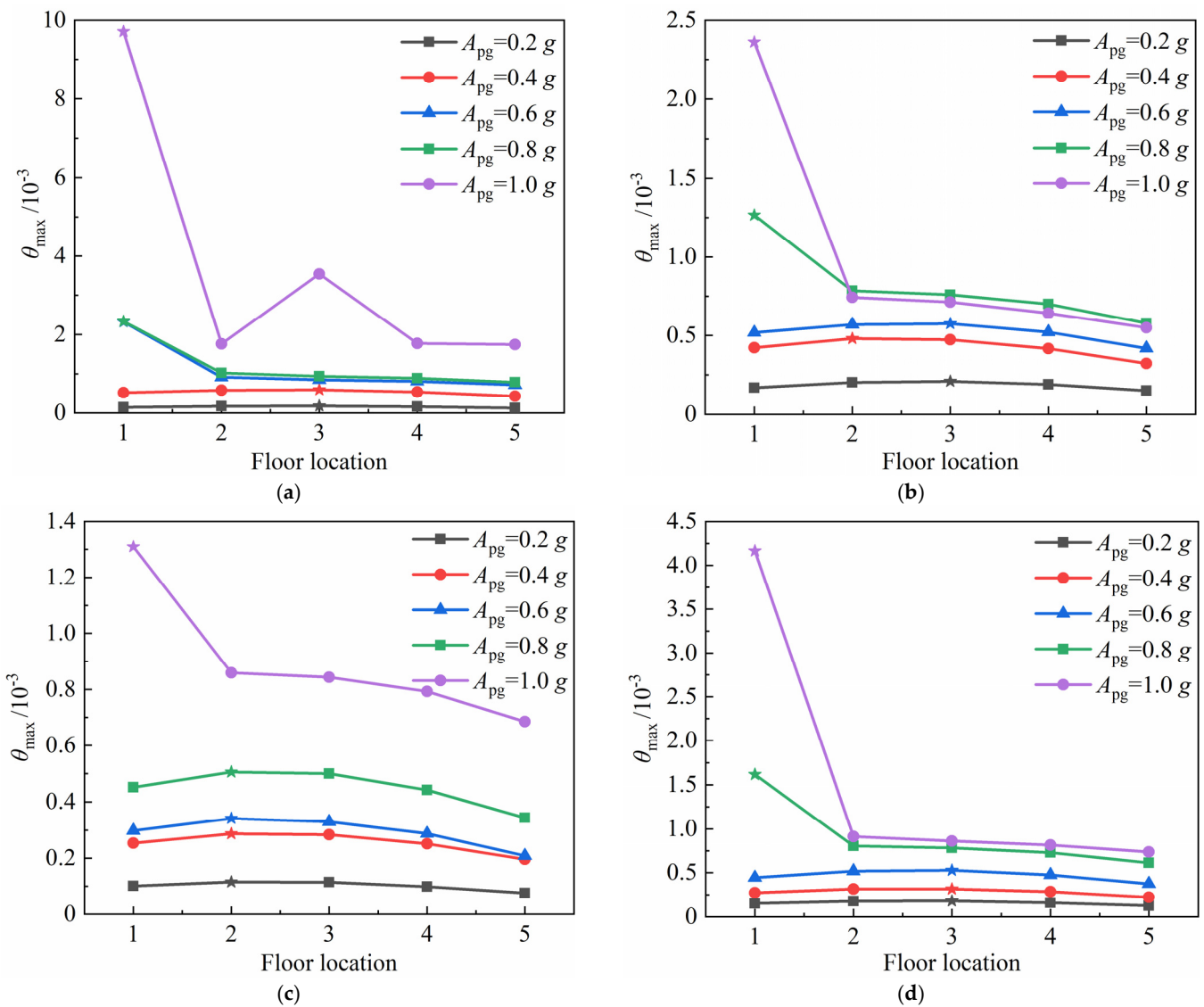
**Figure 11.** IDA curves under earthquake: (a) IDA curves under 20 ground motion records; (b) 16%, 50%, and 84% exceedance probability curves.

Figure 12 shows the maximum inter-story displacement angle and the location of the floor under four groups of ground motion records to obtain the complete development of the inter-story displacement angle of the calculation model. A pentagram demonstrates the floor in Figure 12, where the maximum inter-story displacement angle was located. It was found that when the peak ground acceleration was small, the maximum inter-story displacement angle of the calculation model mainly appeared on the 2nd and 3rd floors. On the other hand, when the peak ground acceleration was large, the maximum inter-story displacement angle of the calculation model mainly appeared on the 1st floor. In particular, with the increase in peak ground acceleration, the inter-story displacement angle became smaller under CAP000. Due to the different spectrum characteristics of ground motion records, the order of development of structural plasticity may differ and the floor location at which the maximum inter-story displacement angle may change accordingly. It is necessary to select a sufficient number of ground motions for the calculation to reflect the weakness of a structure in IDA fully.

It is worth noting that under various ground motion records, the IDA curves are discrete. In order to accurately reflect the seismic capacity of the model under different ground motion records, vulnerability curves can be drawn based on the IDA results. Through the structural failure probability, it may assess its seismic performance and reduce discreteness. The seismic vulnerability curves are generated using the maximum inter-story displacement angle and peak ground acceleration obtained in the previous IDA. According to Mackie's study [53], the maximum inter-story displacement angle ( $\theta_{max}$ ) can be calculated by a power model, which can be expressed as in Equation (4), where  $a$  and  $b$  are the linear regression coefficients. According to the IDA results, the probabilistic structure demand model can be obtained by a linear regression analysis based on Equation (4), as is depicted in Equation (5) and Figure 13.

$$\theta_{max} = aA_{pg}^b \quad (4)$$

$$\ln(\theta_{max}) = -6.12341 + 1.74557 \ln(A_{pg}) \quad (5)$$



**Figure 12.** Inter-story displacement angle under 4 groups ground motion records: (a) DLT352; (b) CAP000; (c) MUL279; (d) CHY101E.

According to Hwang's recommendations [54], structure demand and capacity parameters followed the lognormal distributions. The failure probability of structure demand exceeding the structure capacity  $P_f$  can be expressed as:

$$P_f = \varphi \left[ \frac{\ln(\hat{\theta}) - \ln(\hat{C})}{\sqrt{\beta_c^2 + \beta_d^2}} \right] \quad (6)$$

where  $\hat{\theta}$  and  $\beta_d$  are the mean value and logarithmic standard deviation of the structure demand parameter,  $\hat{C}$  and  $\beta_c$  are the mean value and logarithmic standard deviation of the structural capacity parameter, which could be determined from the performance level points in Table 4. According to Schneider's study [47], when  $A_{pg}$  was used as the independent variable of vulnerability curves,  $\sqrt{\beta_c^2 + \beta_d^2}$  could be taken as 0.5. In addition,  $\varphi(x)$  the standard normal distribution could be described as Equation (7).

$$\varphi(x) = \frac{1}{\sqrt{2\pi}} \int_{-\infty}^x \exp\left(-\frac{t^2}{2}\right) dt \quad (7)$$

Based on Equations (5) and (6), it was possible to determine the failure probability of the maximum inter-story displacement angle reaching each performance level under different ground motion intensities, as demonstrated in Figure 14.

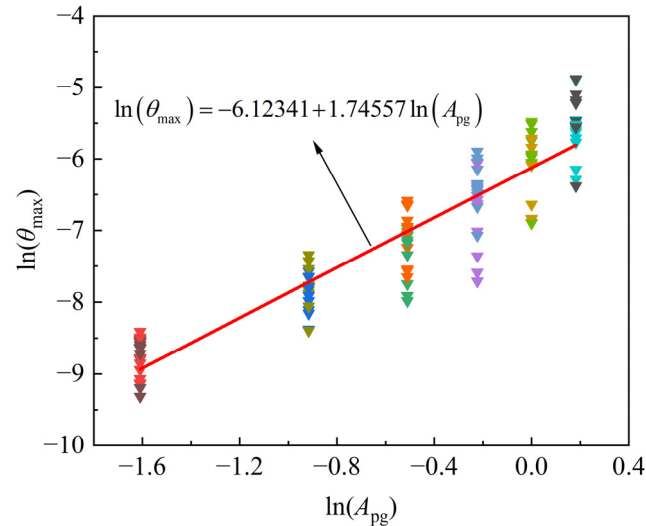


**Figure 13.** The probabilistic structure demand model.

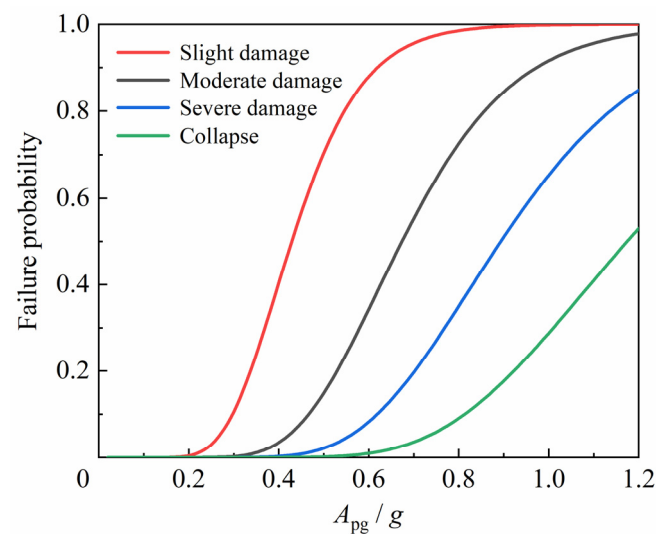


**Figure 14.** Vulnerability curves.

The slope of vulnerability curves was notably different under different performance levels, according to investigations on vulnerability curve characteristics. The slope of vulnerability curves was progressively slower from the operational level (OP) to the collapse prevention level (CP). The vulnerability matrix of the calculation model under 7- and 8-degree earthquakes is shown in Table 5.

It can be seen from Table 5 that the failure probability under the rare earthquake of 8 degrees (0.4 g) at the performance levels of OP to CP was noted as 40.37%, 3.43%, 0.25%, and 0%, respectively. In general, the seismic performance of the model structure under earthquake action was relatively good. Under a rare earthquake, the structure may be moderately damaged; however, the failure probability is not very large; thus, the structure will not be seriously damaged or even collapse. The brick masonry structure was mainly anti-seismic by the wall pieces when the intensity of the ground motion was minimal. With the increase in ground motion intensity, the structural column gradually played a role after the structure cracks, especially when the structure entered a more serious damage

state, such as serious damage and collapse. Small spacing and a robust restraining effect provided by the MSBD structural columns significantly improve the structure's ductility and contribute to preventing the structure from collapsing.

**Table 5.** Vulnerability matrix.

Design Intensity		The Failure Probability under Different Performance Levels			
		Slight Damage	Moderate Damage	Severe Damage	Collapse
7 degree	Frequent earthquake	0	0	0	0
	Design-based earthquake	0	0	0	0
	Rare earthquake	0.99	0	0	0
8 degree	Frequent earthquake	0	0	0	0
	Design-based earthquake	0.39	0	0	0
	Rare earthquake	40.37	3.43	0.25	0

## 5. Conclusions

In the current study, the operation methods of disassembling the brick wall pieces into brick wall sections and building masonry structures with DBWSs were proposed, providing a new choice for reusing masonry structural elements. To evaluate the seismic performance of MSBD, the FEM was established based on Abaqus, and the FEM results were compared with an experimental model to verify the accuracy and practicality of the modeling method. The 20 ground motion records were selected and scaled by peak acceleration in 0.2 g steps to form 120 structure–ground vibration samples for incremental dynamic and seismic vulnerability analysis. The research can provide a reference for seismic design and earthquake damage evaluation of MSBD, which promote the application of DBWSs in building masonry structures. The following conclusions can be drawn from the obtained findings:

(1) The FEM captures the experimental model's stiffness, strength, and ductility with acceptable accuracy, proving the material constitution's applicability and assumptions used in finite element modeling. This modeling method can be regarded as an effective and reliable tool for seismic vulnerability analysis of MSBD.

(2) Based on elastic–plastic analysis under various ground motions, it is possible to determine the progression of a structure from elastic deformation to plastic deformation and ultimately to collapse under an earthquake. From the IDA curves of the calculation model, it can be seen that the maximum inter-story displacement angle increased with the gradual increase in peak ground acceleration. The damage degree gradually increased, the stiffness gradually decreased, and the model transitioned from the elastic stage to the elastoplastic stage.

(3) Due to the different spectrum characteristics of ground motion records, the order of structural plasticity development will be different, and the factor of floors needs to be considered in the seismic performance assessment. To completely reflect the weakness of the structure, a sufficient number of ground motions need to be selected for IDA.

(4) From the seismic vulnerability curves of the calculation model, it can be seen that the structure would not collapse under the 7 and 8 degree design-based earthquake and the probability of moderate and severe damage of the structure under the rare earthquake was also minimal. The structure fulfills the requirements for “no collapse subjected to rare earthquake”. The seismic performance evaluation of structures can use the probabilistic statistics-based seismic vulnerability analysis as a reference.

**Author Contributions:** Conceptualization, Z.S. and W.Z.; methodology, Z.S. and W.Z.; software, Z.S.; validation, Z.S. and Y.W.; formal analysis, Z.S.; investigation, Z.S.; resources, W.Z.; data curation, Z.S.; writing—original draft preparation, Z.S.; writing—review and editing, Y.W. and X.H.; visualization, Z.S.; supervision, Y.W. and X.H.; project administration, W.Z.; funding acquisition, W.Z. All authors have read and agreed to the published version of the manuscript.

**Funding:** This research was funded by Nation Key Research and Development Program of China (Grant No. 2017YFC0806104) and Heilongjiang Touyan Innovation Team Program (Grant No. 2019–49).

**Institutional Review Board Statement:** Not applicable.

**Informed Consent Statement:** Not applicable.

**Data Availability Statement:** The data presented in this study are available on request from the corresponding author. The data are not publicly available as the data contain confidential information, which cannot be publicly disclosed.

**Conflicts of Interest:** The authors declare no conflict of interest.

## References

1. National Development and Reform Commission. Opinions on further work to ban the use of solid clay bricks. *Energy Conserv. Environ. Prot.* **2004**, *3–4*, 6.
2. Zhong, X.; Chen, X. Demolition, rehabilitation, and conservation: Heritage in Shanghai’s urban regeneration, 1990–2015. *J. Archit. Urban.* **2017**, *41*, 82–91. [CrossRef]
3. Lauritzen, E.K. Third International RILEM Symposium on Demolition and Reuse of Concrete and Masonry Odense, Denmark, 24–27 October 1993. *Mater. Struct.* **1994**, *27*, 307–310. [CrossRef]
4. Ghisellini, P.; Ji, X.; Liu, G.; Ulgiati, S. Evaluating the transition towards cleaner production in the construction and demolition sector of China: A review. *J. Clean. Prod.* **2018**, *195*, 418–434. [CrossRef]
5. Kasai, Y. The Second International RILEM Symposium on demolition and reuse of concrete and masonry. *Mater. Struct.* **1989**, *22*, 312–319.
6. Elias Özkan, S. Deconstruction of earthquake damaged buildings in Turkey. In Proceedings of the Deconstruction and Materials Reuse—11th Rinker International Conference on Deconstruction and Materials Reuse, Gainesville, FL, USA, 7–10 May 2003; pp. 138–150.
7. Lieder, M.; Rashid, A. Towards circular economy implementation: A comprehensive review in context of manufacturing industry. *J. Clean. Prod.* **2016**, *115*, 36–51. [CrossRef]
8. Ige, O.; Danso, H. Physico-mechanical and thermal gravimetric analysis of adobe masonry units reinforced with plantain pseudo-stem fibres for sustainable construction. *Constr. Build. Mater.* **2021**, *273*, 121686. [CrossRef]
9. Brick Development Association, BDA Comment on the Use of Reclaimed Clay Bricks. Available online: <https://www.brick.org.uk/admin/resources/g-reclaimed-brickwork.pdf> (accessed on 1 March 2022).
10. Liu, S.; Dai, R.; Cao, K.; Gao, Z. The role of sintered clay brick powder during the hydration process of cement pastes. *Iran. J. Sci. Technol. Trans. Civ. Eng.* **2017**, *41*, 159–165. [CrossRef]
11. Rahhal, V.F.; Trezza, M.A.; Tironi, A.; Castellano, C.C.; Pavlíková, M.; Pokorný, J.; Irassar, E.F.; Jankovský, O.; Pavlík, Z. Complex characterization and behavior of waste fired brick powder-portland cement system. *Materials* **2019**, *12*, 1650. [CrossRef]
12. Phooey Architects, Cubo House. Available online: <http://www.phooey.com.au/projects/90/cubo-house> (accessed on 3 April 2022).
13. Zhou, K.; Chen, H.-M.; Wang, Y.; Lam, D.; Ajayebi, A.; Hopkinson, P. Developing advanced techniques to reclaim existing end of service life (EoSL) bricks—An assessment of reuse technical viability. *Dev. Built Environ.* **2020**, *2*, 100006. [CrossRef]
14. Ucer, D.; Ulybin, A.; Zubkov, S.; Elias-Ozkan, S.T. Analysis on the mechanical properties of historical brick masonry after machinery demolition. *Constr. Build. Mater.* **2018**, *161*, 186–195. [CrossRef]
15. Dolce, M.; Kappos, A.; Zuccaro, G.; Coburn, A. Report of the EAEE Working Group 3: Vulnerability and risk analysis. In Proceedings of the 10th European Conference on Earthquake Engineering, Vienna, Austria, 28 August–2 September 1994; pp. 3049–3077.
16. Shakya, M.; Varum, H.; Vicente, R.; Costa, A. Seismic vulnerability assessment methodology for slender masonry structures. *Int. J. Archit. Herit.* **2018**, *12*, 1297–1326. [CrossRef]
17. GB 50003-2011; Code for Design of Masonry Structures. Ministry of Housing and Urban-Rural Development of the People’s Republic of China: Beijing, China, 2011.
18. 18CG40+18CJ79-1; Assembled Masonry Wall Construction. China Institute of Building Standard Design & Re-Search: Beijing, China, 2018.
19. Lourenço, P.B. Computations on historic masonry structures. *Prog. Struct. Eng. Mater.* **2002**, *4*, 301–319. [CrossRef]
20. Lourenço, P.J.B.B. Computational Strategies for Masonry Structures. Ph.D. Thesis, Technische Universiteit Delft, Delft, The Netherlands, 1997.

21. Yekrangnia, M.; Mohammadi, M. A new strut model for solid masonry infills in steel frames. *Eng. Struct.* **2017**, *135*, 222–235. [[CrossRef](#)]
22. Ferreira, T.M.; Mendes, N.; Silva, R. Multiscale seismic vulnerability assessment and retrofit of existing masonry buildings. *Buildings* **2019**, *9*, 91. [[CrossRef](#)]
23. Tahmasebinia, F.; Ranzi, G.; Zona, A. Probabilistic three-dimensional finite element study on composite beams with steel trapezoidal decking. *J. Constr. Steel Res.* **2013**, *80*, 394–411. [[CrossRef](#)]
24. Agnihotri, P.; Singhal, V.; Rai, D.C. Effect of in-plane damage on out-of-plane strength of unreinforced masonry walls. *Eng. Struct.* **2013**, *57*, 1–11. [[CrossRef](#)]
25. Yang, W.Z. Constitutive model of masonry under compression. *Build. Struct.* **2008**, *38*, 80–82.
26. Ali, S.S.; Page, A.W. Finite element model for masonry subjected to concentrated loads. *J. Struct. Eng.* **1988**, *114*, 1761–1784. [[CrossRef](#)]
27. Sidoroff, F. Description of anisotropic damage application to elasticity. In *Physical Non-Linearities in Structural Analysis*; Springer: Berlin, Germany, 1981; pp. 237–244.
28. Mohammed, M.S. Finite element analysis of unreinforced masonry walls. *Al-Rafidain Eng. J. (AREJ)* **2010**, *18*, 55–68. [[CrossRef](#)]
29. Lourenço, P.; Rots, J. *Analysis of Masonry Structures with Interface Elements*; Faculty of Civil Engineering, Delft University of Technology: Delft, The Netherlands, 1994.
30. Abdulla, K.F.; Cunningham, L.S.; Gillie, M. Simulating masonry wall behaviour using a simplified micro-model approach. *Eng. Struct.* **2017**, *151*, 349–365. [[CrossRef](#)]
31. Dolatshahi, K.M.; Aref, A.J. Two-dimensional computational framework of meso-scale rigid and line interface elements for masonry structures. *Eng. Struct.* **2011**, *33*, 3657–3667. [[CrossRef](#)]
32. GB/T 50129-2011; Standard for Test Method of Basic Mechanics Properties of Masonry. Ministry of Housing and Urban-Rural Development of the People's Republic of China: Beijing, China, 2011.
33. GB/T 50315-2011; Technical Standard for Site Testing of Masonry Engineering. Ministry of Housing and Urban-Rural Development of the People's Republic of China: Beijing, China, 2011.
34. GB 50010-2010; Code for Design of Concrete Structures. Ministry of Housing and Urban-Rural Development of the People's Republic of China: Beijing, China, 2010.
35. Smith, M. *ABAQUS/Standard User's Manual*, version 6.9; Dassault Systèmes Simulia Corp.: Providence, RI, USA, 2009.
36. Dhanasekar, M.; Haider, W. Explicit finite element analysis of lightly reinforced masonry shear walls. *Comput. Struct.* **2008**, *86*, 15–26. [[CrossRef](#)]
37. Farahani, E.M.; Maalek, S. An investigation of the seismic behavior of a deck-type reinforced concrete arch bridge. *Earthq. Eng. Eng. Vib.* **2017**, *16*, 609–625. [[CrossRef](#)]
38. Medeiros, P.; Vasconcelos, G.; Lourenço, P.B.; Gouveia, J. Numerical modelling of non-confined and confined masonry walls. *Constr. Build. Mater.* **2013**, *41*, 968–976. [[CrossRef](#)]
39. Yekrangnia, M.; Bakhshi, A.; Ghannad, M.A. Force-displacement model for solid confined masonry walls with shear-dominated failure mode. *Earthq. Eng. Struct. Dyn.* **2017**, *46*, 2209–2234. [[CrossRef](#)]
40. Dolatshahi, K.M.; Aref, A.J.; Yekrangnia, M. Bidirectional behavior of unreinforced masonry walls. *Earthq. Eng. Struct. Dyn.* **2014**, *43*, 2377–2397. [[CrossRef](#)]
41. Dolatshahi, K.M.; Yekrangnia, M. Out-of-plane strength reduction of unreinforced masonry walls because of in-plane damages. *Earthq. Eng. Struct. Dyn.* **2015**, *44*, 2157–2176. [[CrossRef](#)]
42. Dolsek, M. Incremental dynamic analysis with consideration of modeling uncertainties. *Earthq. Eng. Struct. Dyn.* **2009**, *38*, 805–825. [[CrossRef](#)]
43. Riddell, R.; Garcia, J.E. Hysteretic energy spectrum and damage control. *Earthq. Eng. Struct. Dyn.* **2001**, *30*, 1791–1816. [[CrossRef](#)]
44. GB 50011-2010; Code for Seismic Design of Buildings. Ministry of Housing and Urban-Rural Development of the People's Republic of China: Beijing, China, 2010.
45. FEMA, P. *Quantification of Building Seismic Performance Factors*; US Department of Homeland Security: Washington, DC, USA, 2009.
46. Riahi, Z.; Elwood, K.J.; Alcocer, S.M. Backbone model for confined masonry walls for performance-based seismic design. *J. Struct. Eng.* **2009**, *135*, 644–654. [[CrossRef](#)]
47. Schneider, P.J.; Schauer, B.A. HAZUS—Its development and its future. *Nat. Hazards Rev.* **2006**, *7*, 40–44. [[CrossRef](#)]
48. Seminar, C. *NEHRP Guidelines for the Seismic Rehabilitation of Buildings (FEMA 273)*; Building Seismic Safety Council: Washington, DC, USA, 1997.
49. Cao, X.-Y.; Feng, D.-C.; Li, Y. Assessment of various seismic fragility analysis approaches for structures excited by non-stationary stochastic ground motions. *Mech. Syst. Signal Process.* **2023**, *186*, 109838. [[CrossRef](#)]
50. Pasticier, L.; Amadio, C.; Fragiaco, M. Non-linear seismic analysis and vulnerability evaluation of a masonry building by means of the SAP2000 V. 10 code. *Earthq. Eng. Struct. Dyn.* **2008**, *37*, 467–485. [[CrossRef](#)]
51. Ruiz-García, J.; Miranda, E. Inelastic displacement ratios for evaluation of existing structures. *Earthq. Eng. Struct. Dyn.* **2003**, *32*, 1237–1258. [[CrossRef](#)]
52. Cao, X.-Y.; Feng, D.-C.; Wang, Z.; Wu, G. Parametric investigation of the assembled bolt-connected buckling-restrained brace and performance evaluation of its application into structural retrofit. *J. Build. Eng.* **2022**, *48*, 103988. [[CrossRef](#)]

- 
53. Mackie, K.R.; Stojadinović, B. *Fragility Basis for California Highway Overpass Bridge Seismic Decision Making*; Pacific Earthquake Engineering Research Center, College of Engineering, University of California: Berkeley, CA, USA, 2005.
  54. Hwang, H.; Liu, J.B.; Chiu, Y.-H. *Seismic Fragility Analysis of Highway Bridges*; Center for Earthquake Research and Information, The University of Memphis: Memphis, TN, USA, 2001.